

# Rapid evaluation of notch stress intensity factors using the peak stress method: Comparison of commercial finite element codes for a range of mesh patterns

G. Meneghetti<sup>1</sup> | A. Campagnolo<sup>1</sup> | M. Avalle<sup>2</sup> | D. Castagnetti<sup>3</sup> | M. Colussi<sup>4</sup> | P. Corigliano<sup>5</sup> | M. De Agostinis<sup>6</sup> | E. Dragoni<sup>3</sup> | V. Fontanari<sup>7</sup> | F. Frendo<sup>8</sup> | L. Goglio<sup>9</sup> | G. Marannano<sup>10</sup> | G. Marulo<sup>8</sup> | F. Moroni<sup>11</sup> | A. Pantano<sup>10</sup> | A. Rebori<sup>2</sup> | A. Scattina<sup>9</sup> | A. Spaggiari<sup>3</sup> | B. Zuccarello<sup>10</sup>

<sup>1</sup>Department of Industrial Engineering, University of Padova, Via Venezia, 1-35131 Padova, Italy

<sup>2</sup>Department of Mechanical, Energy, Management and Transportation Engineering, University of Genova, Via all'Opera Pia, 15-16145 Genoa, Italy

<sup>3</sup>Department of Sciences and Methods for Engineering, University of Modena and Reggio Emilia, Via Amendola, 2-42122 Reggio Emilia, Italy

<sup>4</sup>Department of Management and Engineering, University of Padova, Stradella San Nicola, 3-36100 Vicenza, Italy

<sup>5</sup>Engineering Department, University of Messina, Contrada di Dio - 98166 Sant'Agata, Messina, Italy

<sup>6</sup>Department of Industrial Engineering, University of Bologna, Viale del Risorgimento, 2-40136 Bologna, Italy

<sup>7</sup>Department of Industrial Engineering, University of Trento, Via Sommarive, 9 - 38123 Povo, Trento, Italy

<sup>8</sup>Department of Civil and Industrial Engineering, University of Pisa, Largo L. Lazzarino, 2-56122 Pisa, Italy

<sup>9</sup>Department of Mechanical and Aerospace Engineering, Politecnico di Torino, Corso Duca degli Abruzzi, 24-10129 Torino, Italy

<sup>10</sup>Department of Industrial and Digital Innovation, University of Palermo, Viale delle Scienze, 90128 Palermo, Italy

<sup>11</sup>Department of Engineering and Architecture, University of Parma, Via G. P. Usberti 181/A, 43124 Parma, Italy

## Correspondence

G. Meneghetti, Department of Industrial Engineering, University of Padova, Via Venezia, 1-35131 Padova, Italy.  
Email: giovanni.meneghetti@unipd.it

## Abstract

The peak stress method (PSM) is an engineering, finite element (FE)-oriented method to rapidly estimate the notch stress intensity factors by using the singular linear elastic peak stresses calculated from coarse FE analyses. The average element size adopted to generate the mesh pattern can be chosen arbitrarily within a given range.

**Nomenclature:**  $a$ , characteristic size of the analysed sharp V-notch;  $d$ , average size of a finite element mesh;  $e_1, e_2$ , parameters for the evaluation of the averaged strain energy density (SED);  $E$ , elastic modulus;  $f_{w1}, f_{w2}$ , weight parameters of the peak stresses;  $K_1, K_2$ , mode I and II notch stress intensity factors (NSIFs);  $K_{FE}^*, K_{FE}^{**}$ , non-dimensional  $K_1$  and  $K_2$  relevant to the peak stress method (PSM);  $R_0$ , radius of the control volume for the averaged SED evaluation;  $r, \theta$ , polar coordinates;  $u_x, u_y$ , displacement components in the Cartesian frame of reference;  $\bar{W}$ , strain energy density averaged over the control volume;  $x, y$ , Cartesian coordinates

**Symbols:**  $2\alpha$ , opening angle;  $\Delta$ , range of the considered quantity;  $\lambda_1, \lambda_2$ , mode I and mode II eigenvalues in Williams' equation;  $\nu$ , Poisson's ratio;  $\sigma_{I,peak}$ , singular, linear elastic maximum principal stress evaluated at a V-notch tip by FEM using the mesh according to the PSM;  $\sigma_{eq,peak}$ , linear elastic equivalent peak stress evaluated at a V-notch tip;  $\sigma_{ij,c}^{(A)}$ , centroidal stress component in element  $A$ ;  $\sigma_{ij,k}^{(A)}$ , stress component, referred to node  $k$  of element  $A$ ;  $\sigma_{ij,k}$ , stress component, referred to node  $k$ ;  $\sigma_{nom}$ , applied nominal stress;  $\sigma_{\theta\theta}, \tau_{r\theta}$  normal and shear stress components in the polar frame of reference;  $\sigma_{yy,peak}$ , singular, linear elastic, opening peak stress evaluated at a V-notch tip by FEM according to the PSM;  $\tau_{II,peak}, \tau_{xy,peak}$ , singular, linear elastic, sliding peak stress evaluated at the crack tip by FEM according to the PSM;  $[\sigma]_k^{(A)}$ , stress tensor, referred to node  $k$  of element  $A$ ;  $[\sigma]_k$ , stress tensor, referred to node  $k$

**Abbreviations:** FE, finite element; FEM, finite element method; NSIF, notch stress intensity factor; PSM, peak stress method; SED, strain energy density; SIF, stress intensity factor

Originally, the PSM has been calibrated under pure mode I and pure mode II loadings by means of Ansys FE software. In the present contribution, a round robin between 10 Italian universities has been carried out to calibrate the PSM with 7 different commercial FE codes. To this aim, several 2-dimensional mode I and mode II problems have been analysed independently by the participants. The obtained results have been used to calibrate the PSM for given stress analysis conditions in (i) FE software, (ii) element type and element formulation, (iii) mesh pattern, and (iv) criteria for stress extrapolation and principal stress analysis at FE nodes.

**KEYWORDS**

coarse mesh, finite element (FE) analysis, notch stress intensity factor (NSIF), peak stress method (PSM)

**1 | INTRODUCTION**

In plane problems, the local linear elastic stress fields close to the tip of sharp V-notches, like those shown in **FIG 1** the welded joint of Figure 1, can be expressed as functions of the relevant notch stress intensity factors (NSIFs), which quantify the magnitude of the asymptotic singular stress distributions, according to the original analysis performed by Williams<sup>1</sup> under mode I (opening) and mode II (sliding) stresses. The mode I and mode II NSIFs can be defined according to Gross and Mendelson<sup>2</sup> by means of Equations 1 and 2, respectively (see Figure 1B).

$$K_1 = \sqrt{2\pi} \cdot \lim_{r \rightarrow 0} [(\sigma_{\theta\theta})_{\theta=0} \cdot r^{1-\lambda_1}] \quad (1)$$

$$K_2 = \sqrt{2\pi} \cdot \lim_{r \rightarrow 0} [(\tau_{r\theta})_{\theta=0} \cdot r^{1-\lambda_2}] \quad (2)$$

In previous expressions,  $\lambda_1$  and  $\lambda_2$  are the stress singularity exponents,<sup>1</sup> which depend on the notch opening angle  $2\alpha$ , while the stress components  $\sigma_{\theta\theta}$  and  $\tau_{r\theta}$  are

calculated along the notch bisector line, identified by the angular coordinate  $\theta = 0$  (see Figure 1). Values of  $\lambda_1$  and  $\lambda_2$  for the notch opening angles considered in the present contribution are reported in Table 1.

Notch stress intensity factors (NSIFs) have proved to efficiently correlate the static strength of components made of brittle or quasi-brittle materials and weakened by sharp V-notches,<sup>3-9</sup> as well as the medium and high-cycle fatigue strength of notched components made of structural materials.<sup>10,11</sup> Concerning welded joints, NSIFs have been used to analyse the fatigue strength under both uniaxial<sup>12-17</sup> and multiaxial cyclic loadings.<sup>18</sup> However,

**TABLE 1** Values of notch parameters considered in the present work

$2\alpha$ (deg)	$\lambda_1$	$e_1^a$	$\lambda_2$	$e_2^a$
0	0.500	0.133	0.500	0.340
90	0.544	0.145		
135	0.674	0.118		

<sup>a</sup>Values from Lazzarin and Zambardi.<sup>3</sup>

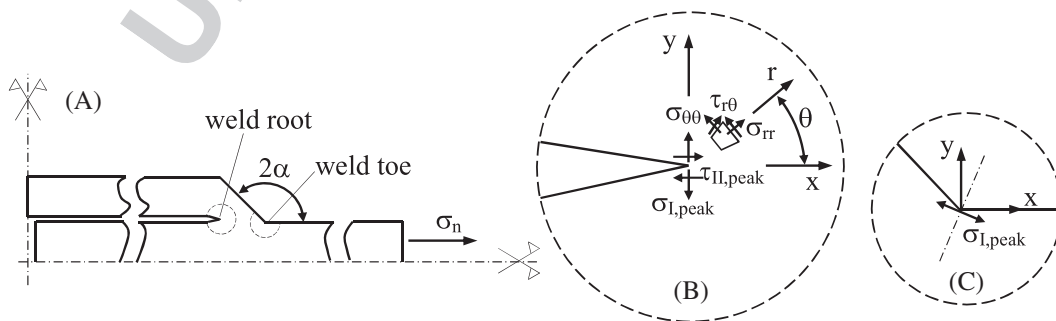


**FIGURE 1** Sharp V-shaped notches in a welded joint A, at the root ( $2\alpha = 0^\circ$ ) B, and at the toe ( $2\alpha$  typically equal to  $135^\circ$ ) C, sides. Definition of peak stresses  $\sigma_{I,peak}$  and  $\tau_{II,peak}$  evaluated at the weld toe and the weld root by means of a linear elastic finite element analysis

calculating the NSIFs by means of finite element (FE) analyses presents a major drawback in engineering problems, because definitions 1 and 2 need very refined FE meshes to evaluate the NSIFs. Finite elements as small as  $10^{-5}$  mm have been adopted in a previous study<sup>14</sup>; in case of 3-dimensional components, numerical analyses could be even more time-consuming.

Recently, a simplified and rapid technique, the so-called peak stress method (PSM), has been proposed to speed up the numerical evaluation of the NSIFs, thanks to FE models with coarse meshes, ie, some orders of magnitude larger than that required to apply definitions 1 and 2. The PSM is based on the numerical procedure proposed by Nisitani and Teranishi<sup>19,20</sup> to rapidly estimate the mode I SIF of a crack emanating from an ellipsoidal cavity. The method has been theoretically justified and extended to estimate also the mode I NSIF of sharp and open V-notches,<sup>21,22</sup> the mode II SIF of cracks,<sup>23</sup> and also the mode III NSIF of open V-notches.<sup>24</sup>

Essentially, the PSM rapidly estimates the NSIFs  $K_1$  and  $K_2$  (Equations 1 and 2) from the singular, linear elastic, opening (mode I) and sliding (mode II) FE peak stresses  $\sigma_{I,peak}$  and  $\tau_{II,peak}$ , respectively, which are calculated at the node located at the V-notch tip (as an example, see Figure 1).

In more detail, the expressions of the PSM are the following<sup>22,23</sup>:

$$K_1 \cong K_{FE}^* \cdot \sigma_{I,peak} \cdot d^{1-\lambda_1} \quad (3)$$

$$K_2 \cong K_{FE}^{**} \cdot \tau_{II,peak} \cdot d^{0.5} \quad (4)$$

In previous relations,  $d$  is the so-called “global element size” parameter adopted by the FE analyst, ie, the average size of the FEs generated by the free mesh generation algorithm available in the numerical code;  $K_{FE}^*$  and  $K_{FE}^{**}$  are nondimensional NSIFs, which must be calibrated to take into account the following parameters of the FE analysis:

- the *element type* and *formulation*
- the *FE mesh pattern*
- the *criteria for stress extrapolation* and *principal stress analysis at FE nodes*

In previously published papers, the PSM has been calibrated by using the Ansys code and the following nondimensional NSIFs have been obtained:  $K_{FE}^* \cong 1.38$  and  $K_{FE}^{**} \cong 3.38$ .<sup>22,23</sup> The conditions of applicability of such nondimensional NSIFs will be summarized in the next paragraph. Besides the much coarser mesh, the PSM has an additional advantage, which is illustrated by

Equations 3 and 4 as compared to previous expressions 1 and 2: only the singular, linear elastic peak stresses evaluated at the V-notch tip are sufficient, instead of a number of *stress-distance* numerical results.

Any structural strength assessment criterion, which is based on NSIF parameters, can in principle be reformulated by using the PSM, thanks to Equations 3 and 4. In the recent literature, the PSM has been coupled to the averaged strain energy density (SED) fatigue criterion to assess the fatigue strength of welded joints subjected to axial<sup>23,25-27</sup> and torsion<sup>24</sup> loading conditions. An example of such application will be given in the next paragraph.

To extend the use of the PSM in practical engineering problems, it is of paramount importance to calibrate the parameters  $K_{FE}^*$  (Equation 3) and  $K_{FE}^{**}$  (Equation 4) by using commercial FE codes different from Ansys. Therefore, a round robin between some Italian universities has been carried out to fill this gap, ie, to check whether or not the parameters  $K_{FE}^* \cong 1.38$  and  $K_{FE}^{**} \cong 3.38$ , previously calibrated by using Ansys, can be used also with other software packages. Possibly, parameters  $K_{FE}^*$  and  $K_{FE}^{**}$  must be updated. It should be noted that to the best of authors' knowledge, some attempts to apply the PSM by adopting FE codes other than Ansys have already been reported in recent contributions by Ranieri et al,<sup>28</sup> who analysed the fatigue strength of steel butt-welded joints according to the PSM by using Adina®, and by Ferro et al,<sup>29</sup> who adopted Sysweld® to rapidly estimate the residual NSIFs again in steel butt-welded joints. However, in these contributions, no systematic calibration of the PSM has been carried out for the adopted FE code. In the present paper, the PSM has been applied to sharp V-notches with different opening angles under pure mode I and cracks under pure mode II loadings by adopting different FE codes. After having calculated the peak stresses, the nondimensional ratios  $K_{FE}^*$  and  $K_{FE}^{**}$  have been evaluated according to Equations 3 and 4, but now expressed in the following fashion:

$$K_{FE}^* \cong \frac{K_1}{\sigma_{I,peak} \cdot d^{1-\lambda_1}} \quad (5)$$

$$K_{FE}^{**} \cong \frac{K_2}{\tau_{II,peak} \cdot d^{0.5}} \quad (6)$$

For each FE software used, the calibration has been performed for fixed stress analysis conditions in (i) element type and element formulation, (ii) mesh pattern, and (iii) criteria for stress extrapolation and principal stress analysis at FE nodes.

## 2 | CALIBRATING THE PEAK STRESS METHOD WITH ANSYS® FINITE ELEMENT CODE

The nondimensional  $K_{FE}^*$  and  $K_{FE}^{**}$  appearing in Equations 3 and 4 have been calibrated in previous contributions,<sup>22,23</sup> to which the reader is referred. Here only a summary of the conditions to apply  $K_{FE}^* \cong 1.38$  and  $K_{FE}^{**} \cong 3.38$  will be reported, according to the following items:

- Element types can be chosen among the next ones available in Ansys element library:
  - two-dimensional, 4-node quadrilateral FEs with linear shape functions (PLANE 42 or alternatively PLANE 182 with K-option 1 set to 3, ie, “*simple enhanced strain*” formulation activated);
  - three-dimensional, 8-node brick elements (SOLID 45 or equivalently SOLID 185 with K-option 2 set to 3, ie, “*simple enhanced strain*” option activated);
  - two-dimensional, harmonic, 4-node linear quadrilateral elements, to analyse axis-symmetric components subjected to external loads that can be expressed according to a Fourier series expansion (PLANE 25).
- The FE mesh pattern close to the notch or crack tip must be that reported in Figure 2 (see also previous

studies<sup>22,23</sup>); in more detail, 4 elements share the node located at the notch tip if the notch opening angle  $2\alpha$  is equal to or lower than  $90^\circ$ , while 2 elements share the node at notch tip when the notch opening angle is  $2\alpha > 90^\circ$ . Figure 2 shows examples of such mesh patterns in case of symmetric FE models. It should be noted that the mesh patterns according to the PSM are automatically generated by the *free-mesh generation algorithm* of Ansys code, after having input the average FE size  $d$  by means of the “global element size” command available in the software. There are no additional parameters or special settings to input to generate the mesh.

- Equation 3 can be applied to sharp V-notches with an opening angle  $2\alpha$  between  $0^\circ$  and  $135^\circ$ , while calibration for mode II loading (Equation 4) is restricted to the crack case ( $2\alpha = 0$ ).
- The average element size  $d$  can be chosen arbitrarily, but within a range of applicability defined in the relevant literature<sup>22,23</sup>: for mode I loading (Equation 3), the mesh density ratio  $a/d$  must exceed 3 to obtain  $K_{FE}^* = 1.38\% \pm 3\%$ ; in case of mode II loading (Equation 4), more refined meshes are needed, the mesh density ratio  $a/d$  having to be greater than 14 to obtain  $K_{FE}^{**} = 3.38\% \pm 3\%$ . The dimension  $a$  is the characteristic size of the analysed sharp V-notch; for example, it is the notch depth in Figure 2. More precisely,  $a$  is the minimum between the notch depth and the

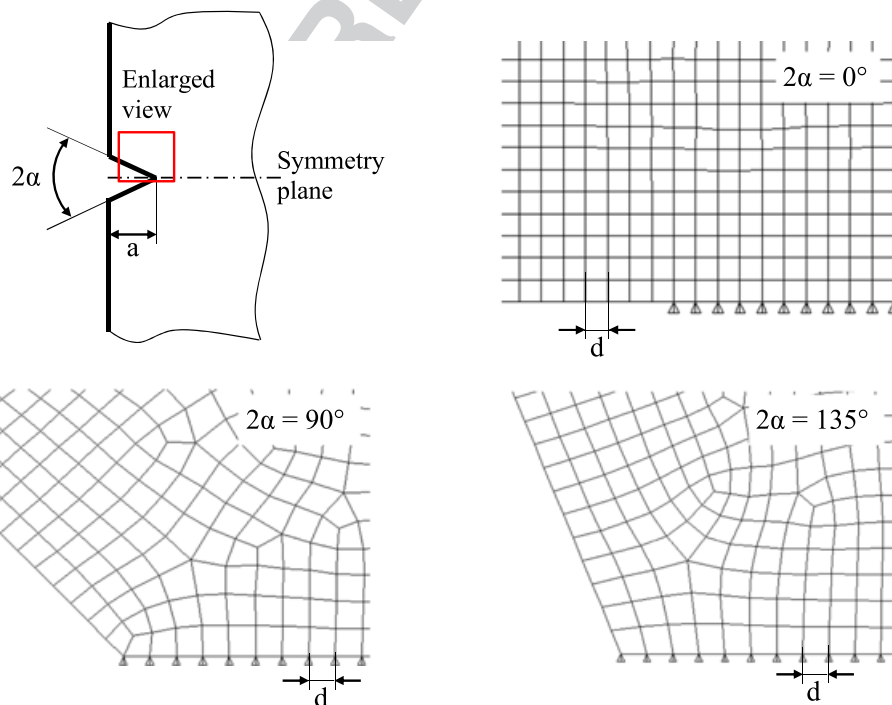


**FIGURE 2** Mesh patterns according to the PSM.<sup>22,23</sup> Symmetry boundary conditions have been applied to the FE model [Colour figure can be viewed at wileyonlinelibrary.com]



ligament size, indicated as  $h$  in the example of next Figure 7, which will be commented later. In all geometries analysed in the present study, the characteristic size  $a$  resulted equal to the notch depth because  $a < h$ . There is only one exception in Table 3 (Figure 7C with  $a = 15$  mm and  $h = 10$  mm) where  $h > a$ ; however, to simplify the presentation of results,  $a$  was kept equal to the notch depth also in this case. The FE size  $d$  has been intentionally taken as the “global element size” input by the FE analyst before running the free mesh generation algorithm available in the FE code. Obviously, the edge lengths of the actually generated FEs will fulfil the prescribed size  $d$  only approximately. Nevertheless, the average FE size  $d$  has been adopted in Equations 3 and 4, the effects of the variability of the FE size in the vicinity of the V-notch tip being included in the scatter band of  $K_{FE}^*$  and  $K_{FE}^{**}$ .

### 3 | A PRACTICAL EXAMPLE: THE PEAK STRESS METHOD APPLIED TO FATIGUE ASSESSMENT OF A WELDED JOINT

To illustrate the PSM in practical design situations, the fatigue strength assessment of conventional arc-welded joints made of structural steel is reported below. Load-carrying cruciform welded steel joints are considered (see the geometry in Figure 3), which were fatigue tested by Ouchida and Nishioka<sup>30</sup> under axial loading. The detailed analysis according to the PSM is reported in Meneghetti

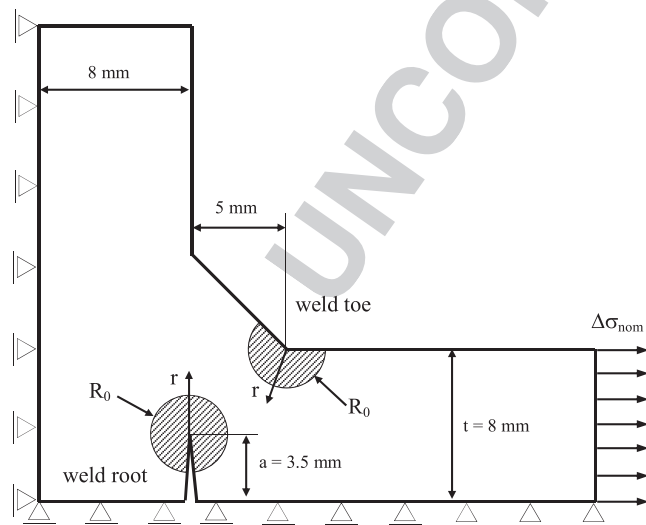


**FIGURE 3** Geometry of the load-carrying steel weld joint tested in Ouchida and Nishioka.<sup>30</sup> Control volumes for the averaged SED evaluation at the weld toe and the weld root sides

and Lazzarin,<sup>31</sup> to which the reader is referred. Only the main steps of the analysis are reported here.

The SED averaged over a structural volume of radius  $R_0$  surrounding the weld root or the weld toe (see Figure 3), as proposed by Lazzarin and co-workers,<sup>3,16</sup> is adopted as fatigue damage parameter. The averaged SED under mode I + II loading can be expressed in closed form as a function of the relevant NSIFs according to Equation 7.

$$\Delta \bar{W} = \frac{e_1}{E} \left( \frac{\Delta K_1}{R_0^{1-\lambda_1}} \right)^2 + \frac{e_2}{E} \left( \frac{\Delta K_2}{R_0^{1-\lambda_2}} \right)^2 \quad (7)$$

where  $R_0$  represents the control radius;  $\Delta K_1$  and  $\Delta K_2$  are the ranges of the NSIFs relevant to mode I and mode II, respectively;  $E$  is the Young's modulus, while  $e_1$  and  $e_2$  are known parameters depending on the notch opening angle  $2\alpha$  and the Poisson's ratio  $\nu$ .<sup>3,16</sup> The size of the structural volume was calibrated on experimental fatigue test data and resulted  $R_0 = 0.28$  mm for welded joints made of structural steel.<sup>16</sup>

Taking advantage of the equality  $W = (1-\nu^2) \cdot \sigma_{eq,peak}^2 / 2E$  valid under plane strain conditions, an equivalent peak stress,  $\sigma_{eq,peak}$ , can be derived as follows<sup>23</sup>:

$$\Delta \sigma_{eq,peak} = \sqrt{\frac{2}{1-\nu^2} \left[ e_1 \left( \frac{\Delta K_1}{R_0^{1-\lambda_1}} \right)^2 + e_2 \left( \frac{\Delta K_2}{R_0^{1-\lambda_2}} \right)^2 \right]} \quad (8)$$

where  $e_1$  and  $e_2$  are known coefficients that depend on the notch opening angle  $2\alpha$  and the Poisson's ratio; values relevant to the present paper are listed in Table 1. If  $\Delta K_1$  and  $\Delta K_2$  are evaluated directly at the weld toe and at the weld root by means of definitions (Equations 1 and 2), the mesh density must be very refined, as reported in Figure 4. After applying definition 1, the mode I NSIFs were determined at the toe and root resulting in  $\Delta K_{1,toe} = 3.40$  MPa mm<sup>0.326</sup> and  $\Delta K_{1,root} = 2.95$  MPa mm<sup>0.5</sup>, respectively, while mode II is not singular at weld toe and it is negligible at weld root in this case ( $\Delta K_{2,root} \approx 0$ ). It is worth noting that Figure 4 reports the nodal stresses; therefore, the minimum element size of  $10^{-5}$  mm adopted in the FE simulation can be appreciated.

By using the PSM-based relationships (Equations 3 and 4), Equation 8 can be rewritten as a function of the singular, linear elastic FE peak stresses  $\sigma_{I,peak}$  and  $\tau_{II,peak}$ <sup>23</sup>:

$$\Delta \sigma_{eq,peak} = \sqrt{f_{w1}^2 \cdot \Delta \sigma_{I,peak}^2 + f_{w2}^2 \cdot \Delta \tau_{II,peak}^2} \quad (9)$$

All parameters appearing in Equations 3, 4, and 8 are included in coefficients  $f_{w1}$  and  $f_{w2}$ , whose expression has been reported in the literature.<sup>23</sup>

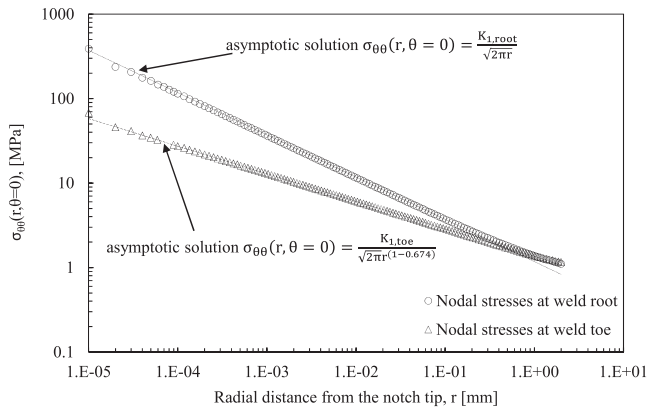


**FIGURE 4** Singular, linear elastic stress fields at the weld toe and the weld root, obtained from very refined FE mesh patterns (minimum FE size  $d_{\min} \approx 10^{-5}$  mm) and comparison with the asymptotic solutions based on the relevant NSIF. The nominal applied stress  $\Delta\sigma_{\text{nom}}$  is equal to 1 MPa

The peak stresses were calculated by using the FE mesh **F5** reported in Figure 5, according to the following steps:

- A 2D FE analysis was performed under plane strain conditions by adopting 4 node quadrilateral elements (PLANE 182 of Ansys element library, with K-option 1 set to 3, ie, “*simple enhanced strain*” formulation activated).
- The mesh density ratio  $a/d$  was established as follows:  $a$  is the precrack length at the root side, so that the maximum FE size  $d$  is equal to  $a/3 = 3.5/3 \rightarrow \approx 1$  mm and is appropriate to apply Equation 9; at the toe side,  $a$  is half the main plate thickness, ie,  $a = 8$  mm; therefore, the maximum FE size is  $8/3 = 2.66$ . In conclusion,  $d = 1$  mm is appropriate both at the root and at the toe side.
- The *free-mesh* pattern (see Figure 5A) was generated by setting a “global element size” parameter  $d = 1$  mm in the free mesh generation algorithm.

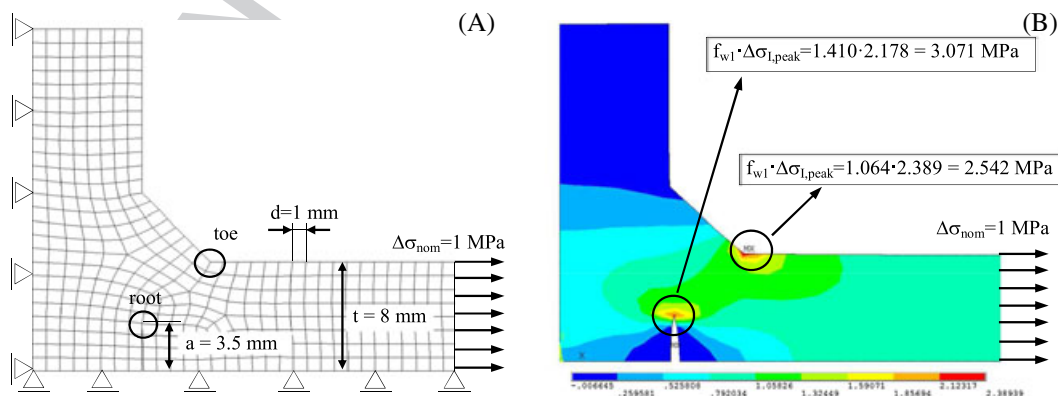


**FIGURE 5** Application of the PSM to the fatigue strength assessment of a load-carrying arc-welded joint made of structural steel and tested in Ouchida and Nishioka<sup>30</sup> [Colour figure can be viewed at wileyonlinelibrary.com]

- The maximum principal stress  $\Delta\sigma_{I,\text{peak}}$  was evaluated at the FE nodes located at the weld toe and root; by using Equation 3, it is obtained  $\Delta K_{I,\text{toe}} \cong 1.38 \cdot 2.389 = 3.30 \text{ MPa mm}^{0.326}$  and  $\Delta K_{I,\text{root}} \cong 1.38 \cdot 2.178 = 3.01 \text{ MPa mm}^{0.5}$ ; both values are in very good agreement with those calculated with very refined meshes by means of definition 1.
- Figure 5B shows the results according to PSM:
  - weld toe side:  $\Delta\sigma_{\text{eq,peak}} \cong f_{w1} \cdot \Delta\sigma_{I,\text{peak}} = 1.064 \cdot 2.389 = 2.54 \text{ MPa}$
  - weld root side:  $\Delta\sigma_{\text{eq,peak}} \cong f_{w1} \cdot \Delta\sigma_{I,\text{peak}} = 1.410 \cdot 2.178 = 3.07 \text{ MPa}$

As a conclusion, according to the PSM, the weld root is more critical than the weld toe, because  $\Delta\sigma_{\text{eq,peak}}$  is higher at the root (3.07 MPa) than at the toe (2.54 MPa). This is in agreement with the fatigue crack initiation point experimentally observed by Ouchida and Nishioka.<sup>30</sup> Subsequently, the original experimental data have been reconverted in equivalent peak stress evaluated at the weld root by means of Equation 9. Finally, Figure 6 **F6** shows the comparison between the experimental results and the fatigue design scatter band previously calibrated in Meneghetti and Lazzarin.<sup>31</sup> A good agreement between theoretical estimations and experimental results can be observed.

#### 4 | PARTICIPANTS AND FINITE ELEMENT CODES INVOLVED IN THE ROUND ROBIN

The participants and the FE codes involved in the round robin are listed in Table 2. Ten universities took **T2** part to the project, and 7 commercial FE codes were calibrated.

Table 2 shows that Optistruct and Ls-Dyna were used to solve the numerical models, while Hypermesh and

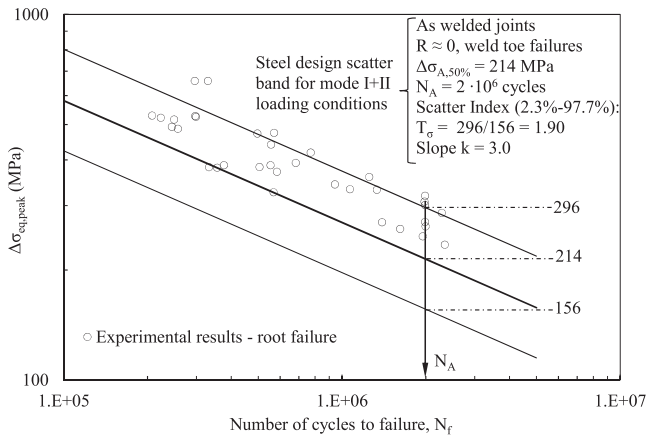


**FIGURE 6** Fatigue assessment of load-carrying steel welded joints according to the PSM. Comparison between the fatigue design scatter band of the PSM<sup>31</sup> and experimental fatigue results from Ouchida and Nishioka<sup>30</sup>

**TABLE 2** List of participants (alphabetic order) and FE codes

Universities (Alphabetical Order)	FE Codes (Alphabetical Order)
Bologna (UNIBO)	Ansys 16 and 17
Genova (UNIGE)	Abaqus 6.13 and 6.14
Messina (UNIME)	Hypermesh 14 <sup>a</sup> /Optistruct 14 implicit/Hyperview 14 <sup>b</sup>
Modena and Reggio Emilia (UNIMORE)	Hypermesh 13 <sup>a</sup> /Ls-Dyna R7.1.3 implicit/Hyperview 13 <sup>b</sup>
Padova (UNIPD)	Lusas 14.6-2
Palermo (UNIPA)	MSC Patran/Nastran 2014 and 2016
Parma (UNIPR)	Straus 7 R.2.4.6
Pisa (UNIPI)	
Politecnico di Torino (POLITO)	
Trento (UNITN)	

<sup>a</sup>Preprocessor.

<sup>b</sup>Postprocessor.

Hyperview were used as preprocessor and postprocessor codes, respectively.

## 5 | GEOMETRIES, MATERIAL, AND FINITE ELEMENT MESH PATTERNS

A number of 2-dimensional geometries subjected to mode I or mode II loading conditions were analysed by using the different FE codes. Geometries involved cracks as well as pointed V-notches and not necessarily reproduce welded joint geometries, because of the general validity of expressions 5 and 6 to be calibrated. Geometries,

material properties, boundary conditions, and FE type were obviously the same in all FE codes involved in the round robin. Conversely, as far as possible, specific options concerning element formulation, free mesh generation algorithms, stiffness matrix inversion algorithms, stress extrapolation, and stress averaging rules at FE nodes have been set to *default options* in each software. Sometimes, with the sole aim to investigate the reasons for different results obtained, the FE mesh pattern generated with a given software has been imported into another software, so that the results could be compared for precisely the same adopted mesh. All details concerning the analyses performed and the obtained results are given in the following.

### 5.1 | 2D problems (plane strain), mode I loading, $0^\circ \leq 2\alpha \leq 135^\circ$

Different geometries subjected to pure mode I as reported in Figure 7 have been considered. All these case studies are the same adopted in the original calibration of the PSM under mode I loading, which was performed by using Ansys FE code.<sup>22</sup> In particular, they consist of the following geometries: a crack located at the U-notch tip (Figure 7A), a crack at the free surface of a finite-width plate (Figure 7B), a plate with lateral open V-notches (Figure 7C), and, finally, a typical full-penetration cruciform welded joint with a weld toe angle equal to  $135^\circ$  (Figure 7D). The material is a structural steel with Young's modulus  $E = 206\,000$  MPa and Poisson's ratio  $\nu = 0.3$ .

To calculate the peak stress values, linear elastic static analyses under plane strain conditions have been carried out and a FE pattern of 4-node linear quadrilateral elements has been used as shown in the examples of Figure 8, which refers to Ansys software. Only a quarter of each model has been analysed by taking advantage of the double symmetry condition. The free mesh generation algorithm was run in each software after setting the average element size  $d$  to adopt. The mesh density ratio  $a/d$  was varied in a wide range by considering either a variation of the notch/crack size  $a$  or a variation of the FE size  $d$ , as reported in Table 3.

All generated meshes were checked to assure that the FE pattern at the notch or crack tip was of the type shown in Figure 2. If the mesh pattern generated by the free mesh generator was not the standard 1 reported in Figure 2 (in a symmetric model, 1 element was sometimes obtained at the notch tip when  $2\alpha = 90^\circ$ , instead of 2, or 2 elements were sometimes obtained when  $2\alpha = 135^\circ$ , instead of one), then mesh generation was repeated by changing slightly the average element size  $d$  up to 10% of the nominal values reported in Table 3 until the

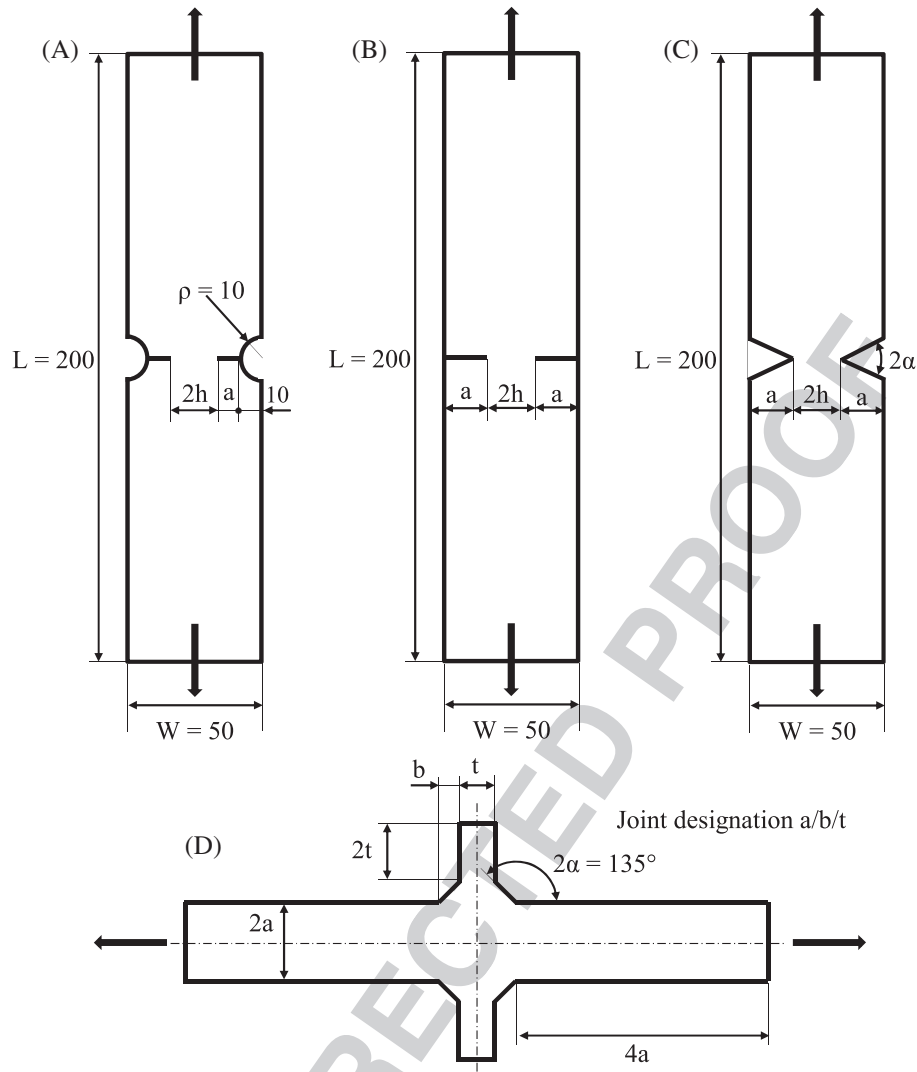


**FIGURE 7** Geometries of 2D problems (plane strain) under mode I loading. Dimensions in [mm]

standard mesh was obtained. In these cases, the actual  $d$  value has been adopted to calculate the ratio  $a/d$  and  $K_{FE}^*$  (Equation 5). Figure 8 highlights that the area of the models has not been divided into subareas. The external load has been applied as a nominal gross-section stress equal to 1 MPa.

After solving the FE model, the peak value of the maximum principal stress  $\sigma_{I,peak}$  was taken at the FE node located at the V-notch tip (see Figure 8). Stress averaging at FE nodes was activated in each FE code, so that only a single stress value for  $\sigma_{I,peak}$  has been obtained per node by averaging the nodal stresses from all elements that share the node. To this end, the default options of each FE code have been used, whenever possible, as it will be explained in detail in the following.

The exact mode I NSIFs  $K_I$ , to input in Equation 5, were derived by using Ansys software and by applying definition 1 to the stress-distance numerical results obtained from very refined FE mesh patterns (the size of

the smallest element close to the V-notch tip was of the order of  $10^{-5}$  mm).

## 5.2 | 2D problems (plane strain), mode II loading, $2\alpha = 0^\circ$

A crack ( $2\alpha = 0^\circ$ ) centred in a plate having the geometry reported in Figure 9 and subjected to pure mode II loading was considered. The case study has been taken from the original calibration of the PSM under mode II loading conditions for Ansys FE code.<sup>23</sup> The considered material is a structural steel with Young's modulus  $E = 206\,000$  MPa and Poisson's ratio  $\nu = 0.3$ .

The peak stresses were calculated by means of linear elastic static analyses under plane strain conditions and a pattern of 4-node linear quadrilateral elements as shown in the example of Figure 10. The mesh density ratio  $a/d$  was varied in a wide range from 1 to 200 as reported in Table 4. Only a quarter of the cracked plate was analysed



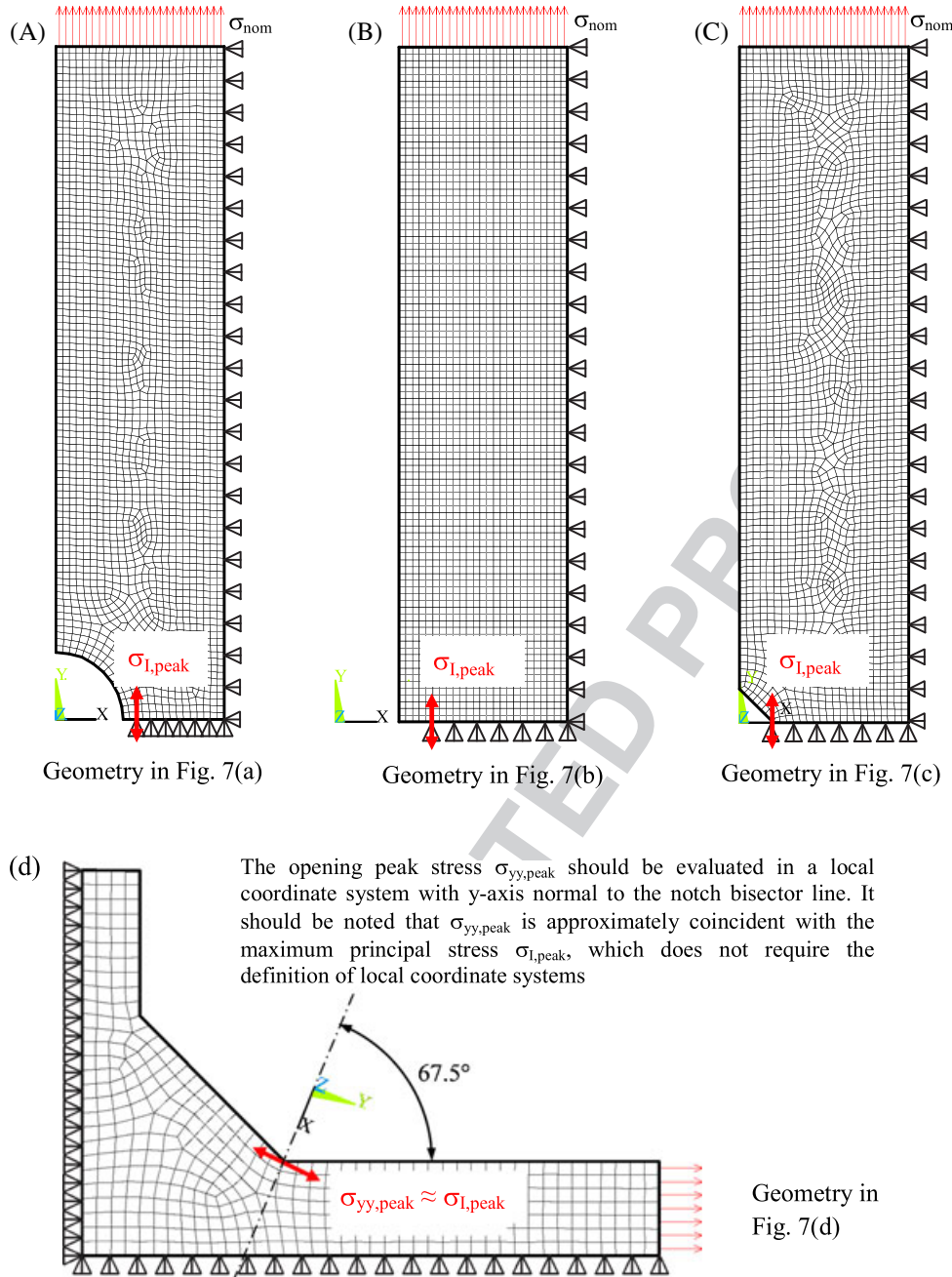


**FIGURE 8** FE mesh patterns and boundary conditions applied into the FE analyses of 2D problems (plane strain) under mode I loading. Geometries are reported in Figure 7. FE patterns shown in the figure have been generated by using Ansys [Colour figure can be viewed at wileyonlinelibrary.com]

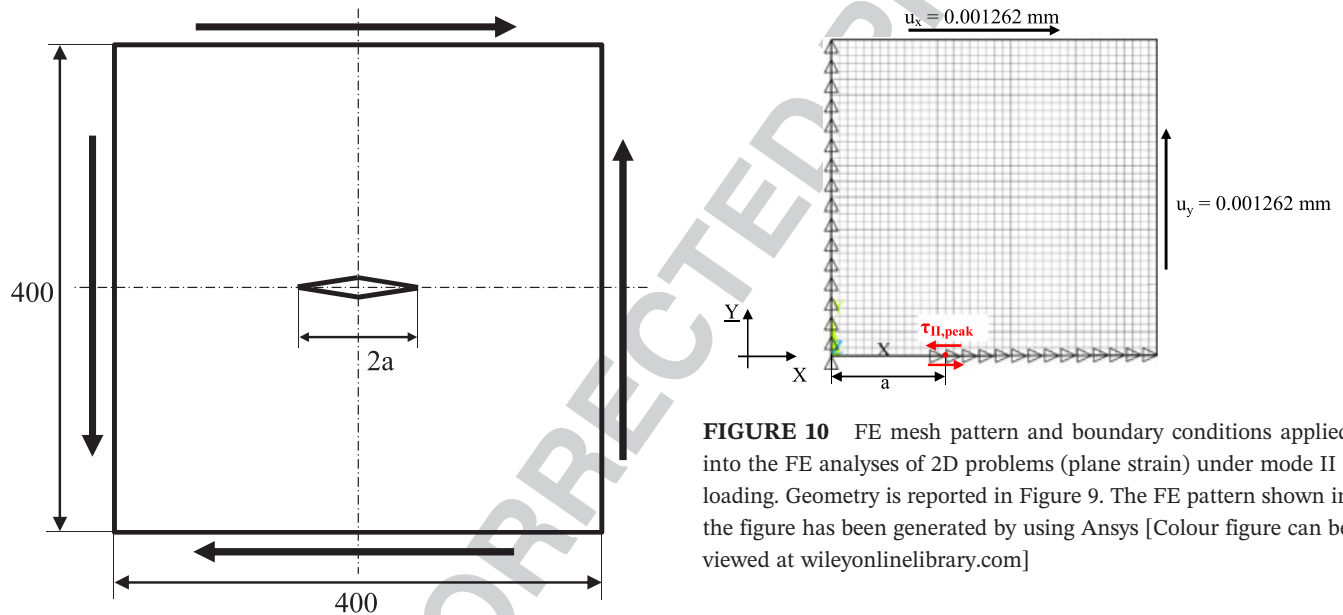
by taking advantage of the double antisymmetry boundary conditions (see Figure 10).

The external load was applied to the FE model by means of displacements  $u_x = u_y = 1.262 \cdot 10^{-3}$  mm at the plate free edges. Such displacements translate into a nominal gross shear stress equal to 1 MPa in absence of the crack, while the presence of the crack alters the shear stress distribution in the gross section. However, the same loading condition in prescribed displacement has been maintained to evaluate the exact SIF  $K_2$  (using extremely

refined FE meshes) as well as to calculate the sliding FE peak stress  $\tau_{II,peak}$  (using coarse meshes according to the PSM). After solving the FE model, the peak value of the (mode II) shear stress  $\tau_{xy,peak} = \tau_{II,peak}$  has been taken at the node located at the crack tip (see Figure 10). Stress averaging at FE nodes has been activated as explained for mode I analyses. Again, the exact mode II SIFs  $K_2$ , to input in Equation 6, were calculated by using Ansys and by applying definition 2 to the stress-distance numerical results obtained from very refined FE mesh patterns (the

**TABLE 3** FE analyses of 2D problems (plane strain) under mode I loading

Analysed Geometries						
Figure	$a$ [mm]	$d$ [mm]	$2\alpha$ [°]	$b$ [mm]	$t$ [mm]	Number of Analyses <sup>a</sup>
7A	1, 2, ... ,9, 10	1	0	-	-	10
7B	1, 2, ... ,19, 20	1	0	-	-	20
7B	10	1, 2, 5, 10	0	-	-	4
7C	10	1, 2.5, 5, 10	135	-	-	4
7C	5	0.5, 1, 2, 2.5, 5	90	-	-	5
7C	10	0.6, 1, 2.5, 3, 5, 7.5	90	-	-	6
7C	15	0.6, 1, 2, 5	90	-	-	4
7C	6.5	1, 1.64, 6.5	135	10	8	3
7C	50	1, 2, 5, 10, 25	135	50	16	5

<sup>a</sup>Total number of analyses: 61.**FIGURE 9** Geometry of 2D problems (plane strain) under mode II loading. Dimensions in [mm]

size of the smallest element close to the crack tip was of the order of  $10^{-5}$  mm).

## 6 | DETAILS OF MESH GENERATION SETTINGS

It has been mentioned that 2-dimensional, 4-node, linear quadrilateral elements under plane strain hypothesis were adopted in the FE analyses. The element was integrated by using  $2 \times 2$  Gauss points. After selecting the proper element type, the average element size  $d$  has been the sole parameter used by the FE analyst, to drive the

**FIGURE 10** FE mesh pattern and boundary conditions applied into the FE analyses of 2D problems (plane strain) under mode II loading. Geometry is reported in Figure 9. The FE pattern shown in the figure has been generated by using Ansys [Colour figure can be viewed at wileyonlinelibrary.com]

automatic free mesh generation algorithm. Specific details concerning element type/options along with the adopted mesh generation settings are reported for each FE code in Appendix A.

## 7 | RESULTS OF FE ANALYSES

The results obtained from the participants to the Round Robin are reported in Figures 11A-G and 12 for mode I and mode II problems, respectively. The figures show the nondimensional ratios  $K_{FE}^*$  and  $K_{FE}^{**}$ , defined in Equations 5 and 6, respectively, as a function of the mesh density ratio  $a/d$ . Results shown in Figures 11A-G and 12 have been obtained with the *default options* of the postprocessing environment, which are listed in Appendix B for the sake of clarity.

**TABLE 4** FE analyses of 2D problems (plane strain) under mode II loading

Analysed Geometries			
$a$ [mm]	$d$ [mm]	$2\alpha$ [°]	Number of Analyses <sup>a</sup>
1	0.5, 1	0	2
2	0.5, 1, 2	0	3
3	0.5, 1, 3	0	3
4	0.5, 1, 2, 4	0	4
5	0.5, 1, 5	0	3
6	0.5, 1, 2, 3	0	4
7	0.5, 1	0	2
8	0.5, 1, 2, 4	0	4
9	0.5, 1, 3	0	3
10	0.5, 1, 2, 5, 10	0	5
20	0.5, 1, 2, 4, 5, 10	0	6
30	0.5, 1, 2, 3, 5, 10, 15	0	7
40	0.5, 1, 2, 4, 5, 10, 20	0	7
50	0.5, 1, 2, 5, 10	0	5
60	0.5, 1, 2, 3, 4, 5, 10, 15, 20	0	9
70	0.5, 1, 2, 5, 10	0	5
80	0.5, 1, 2, 4, 5, 10, 20	0	7
90	0.5, 1, 2, 3, 5, 10, 15	0	7
100	0.5, 1, 2, 4, 5, 10, 20	0	7

<sup>a</sup>Total number of analyses: 93.

Dealing with mode I loading, it can be observed from Figure 11B-E that most of the considered FE codes, ie, Abaqus, Straus 7, MSC Patran/Nastran, and Lusas, present the same parameter  $K_{FE}^* \cong 1.38$  that had been previously calibrated in Ansys<sup>22</sup> and it is reported in Figure 11A. It should be noted that for all FE codes, convergence is achieved for a mesh density ratio  $a/d \geq 3$ , such value being consistent once more with the original calibration.<sup>22</sup> A slightly greater scatter band of  $\pm 5\%$  should instead be accepted, as compared to Meneghetti and Lazzarin<sup>22</sup> where  $\pm 3\%$  was found.

On the other hand, Figure 11F,G shows that the FE packages Hypermesh/Optistruct/Hyperview and Hypermesh/Ls-Dyna/Hyperview present a different calibration constant, ie,  $K_{FE}^* \cong 1.84$ . This peculiar behaviour depends on stress extrapolation rules at FE nodes and will be analysed later on. Moreover, the scatter  $\pm 8\%$  (see Figure 11F,G) is higher as compared to  $\pm 5\%$  obtained with the other FE codes (see Figure 11A,E).

Dealing with mode II loading, Figure 12 reports the results and shows that all considered FE codes converge to  $K_{FE}^{**} \cong 3.38 \pm 3\%$ , ie, the values calibrated previously

for Ansys software.<sup>23</sup> Convergence is achieved for a mesh density ratio  $a/d \geq 14$ , which is consistent with the original calibration.<sup>23</sup>

All results reported in Figures 11 and 12 are summarized in Table 5, which reports the nondimensional ratios  $K_{FE}^*$  and  $K_{FE}^{**}$  to use in Equations 3, 4, and 9 and the minimum mesh density ratio  $a/d$  for all considered FE codes.

## 8 | DISCUSSION

In the previous paragraph, it has been observed that under mode I loading, there are some discrepancies among the results delivered by the different FE codes. As a major discrepancy, Figure 11 and Table 5 show that Hypermesh/Optistruct/Hyperview and Hypermesh/Ls-Dyna/Hyperview converge to  $K_{FE}^* = 1.84$ , while all other FE codes converge to  $K_{FE}^* = 1.38$ . Minor differences in results delivered by the different FE codes also exist, but they are taken up by the scatter bands. Such discrepancies have been explained by examining the different procedures for stress extrapolation and principal stress analysis at FE nodes, mesh patterns adopted by the different FE codes, and numerical integration schemes. Detailed explanations are given in the following.

### 8.1 | Stress extrapolation at finite element nodes

Finite element codes compute results at the integration (or Gauss) points. Afterwards, results can be computed at nodal or centroidal locations, on the basis of the element shape functions. Once the nodal or centroidal stress in the element is obtained, it is possible to calculate the stress at a node shared by more than 1 element according to 2 different procedures, which are sketched in Figure 13:

- The nodal stresses in the element ( $\sigma_{ij,k}^{(A)}$  and  $\sigma_{ij,k}^{(B)}$  in Figure 13A) are extrapolated from the stresses at the integration points. Afterwards, the stress at the shared node ( $\sigma_{ij,k}$  in Figure 13A) is calculated by averaging the nodal stresses per element according to the expression:

$$\sigma_{ij,k} = \frac{\sigma_{ij,k}^{(A)} + \sigma_{ij,k}^{(B)}}{2} \quad (10)$$

- The centroidal stresses in the element ( $\sigma_{ij,c}^{(A)}$  and  $\sigma_{ij,c}^{(B)}$  in Figure 13B) are interpolated from the stresses at the integration points and are attributed to the shared node ( $\sigma_{ij,k}$  in Figure 13B). Then, the

F13

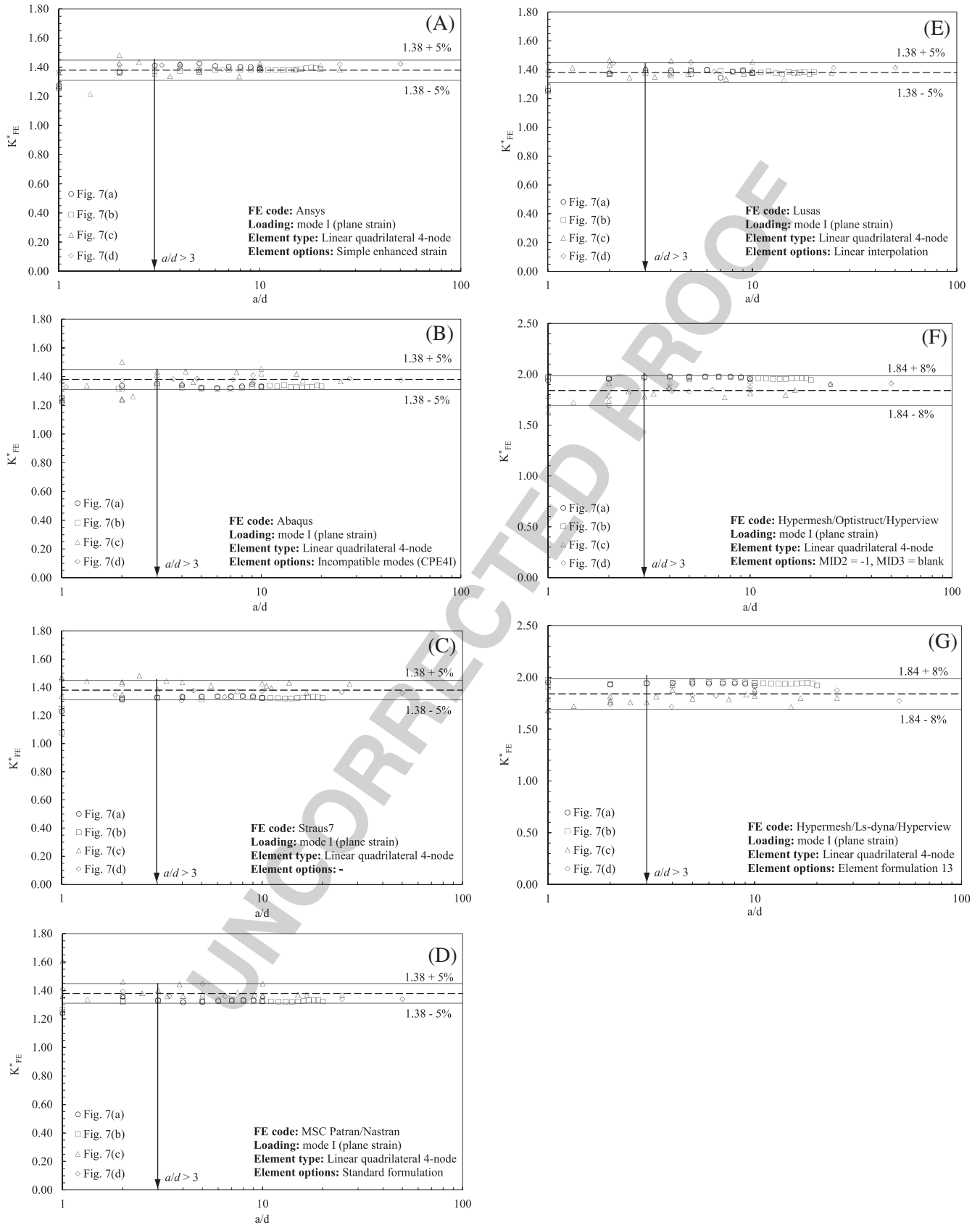
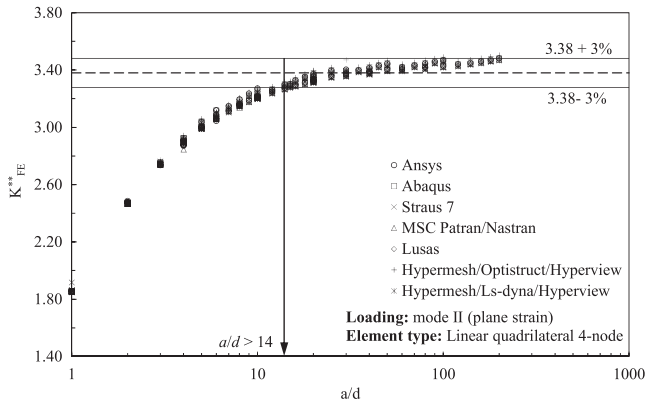


FIGURE 11 Results of round robin for mode I loading: Non-dimensional ratio  $K_{FE}^*$  for each FE code





**FIGURE 12** Results of round robin for mode II loading: Non-dimensional ratio  $K_{FE}^{**}$  for all considered FE codes

stress at the shared node is calculated according to the expression:

$$\sigma_{ij,k} = \frac{\sigma_{ij,c}^{(A)} + \sigma_{ij,c}^{(B)}}{2} \quad (11)$$

It should be noted that stress extrapolation at nodes according to Figure 13A and Equation 10 is carried out by most of the considered FE codes, ie, Ansys, Abaqus, Straus 7, MSC Patran/Nastran, and Lusas. On the other hand, the postprocessor Hyperview allows to adopt either Equation 10 or Equation 11; however, both Optistruct and Ls-Dyna do not calculate the nodal stresses in the element, so that Hyperview can extrapolate stress at nodes only according to Figure 13B and Equation 11. This is the reason why  $K_{FE}^{**}$  obtained with Optistruct and Ls-Dyna (Figure 11F,G) is different from that obtained with the other FE codes (Figure 11A-E).

To support this conclusion, calibration under mode I was repeated by adopting Ansys FE software, but now forcing the use of Equation 11 (see Figure 13B) to calculate the nodal stresses. The obtained results are reported in Figure 14, where it is seen that under these conditions, Ansys converges to the same value  $K_{FE}^{**} \cong 1.84$  reported in Figure 11F,G for Hypermesh/Optistruct/Hyperview and Hypermesh/Ls-Dyna/Hyperview. To mimic these software packages with Ansys as accurately as possible, the averaging option (b) reported in next Table 6, and the full integration option, as reported in next Table 9, were adopted. This point will be clarified when commenting on the relevant tables.

## 8.2 | Principal stress averaging

Whatever the nodal stress evaluation technique (either Equation 10 or Equation 11), the principal stresses at a node shared by more than 1 element can be calculated

**TABLE 5** Results of round robin for mode I and mode II loadings

Software	Element/No. of Nodes	Integration/ Gauss Points	Element Shape	Mesh Generation Technique	$K_{FE}^{**}$ (Equation 5)			$K_{FE}^{**}$ (Equation 6)		
					Value	Opening Angle	Min a/d	Value	Opening angle	Min a/d
Ansys 16 and 17	PLANE 182/4 node	Simple enhanced strain/ $2 \times 2$	Quadrangular	Free-mesh, global element size $d$	$1.38 \pm 5\%$	$0^\circ \leq 2\alpha \leq 135^\circ$	3	$3.38 \pm 3\%$	$0^\circ$	14
Abaqus 6.13 and 6.14	CPE4I/4-node	Incompatible modes/ $2 \times 2$	Quadrangular		$1.38 \pm 5\%$	$0^\circ \leq 2\alpha \leq 135^\circ$	3	$3.38 \pm 3\%$	$0^\circ$	14
Straus 7 R2.4.6	QUAD 4/4-node	Incompatible modes/ $2 \times 2$	Quadrangular		$1.38 \pm 5\%$	$0^\circ \leq 2\alpha \leq 135^\circ$	3	$3.38 \pm 3\%$	$0^\circ$	14
MSC Patran/Nastran 2014 and 2016	CQUAD4/4-node	Standard formulation/ $2 \times 2$	Quadrangular		$1.38 \pm 5\%$	$0^\circ \leq 2\alpha \leq 135^\circ$	3	$3.38 \pm 3\%$	$0^\circ$	14
Lusas 14.6-2	QPN4M/4-node	Full with Enh. Strain/ $2 \times 2$	Quadrangular		$1.38 \pm 5\%$	$0^\circ \leq 2\alpha \leq 135^\circ$	3	$3.38 \pm 3\%$ <sup>a</sup>	$0^\circ$	14
Hypermesh 14/Optistruct 14 implicit/Hyperview 14	Shell 4-node/CQUAD4	$n.a.$ , $2 \times 2$	Quadrangular		$1.84 \pm 8\%$	$0^\circ \leq 2\alpha \leq 135^\circ$	3	$3.38 \pm 3\%$	$0^\circ$	14
Hypermesh 13/LSTC ls-dyna R7.1.3 implicit/Hyperview 13	Shell 4-node/element formulation 13	$n.a.$ , $2 \times 2$	Quadrangular		$1.84 \pm 8\%$	$0^\circ \leq 2\alpha \leq 135^\circ$	3	$3.38 \pm 3\%$	$0^\circ$	14

Mean values of non-dimensional ratios  $K_{FE}^{**}$  and  $K_{FE}^{**}$  and minimum mesh density ratio  $a/d$  for all considered FE codes.

<sup>a</sup>Calibration obtained by adopting mapped-mesh with "global element size"  $d$ .

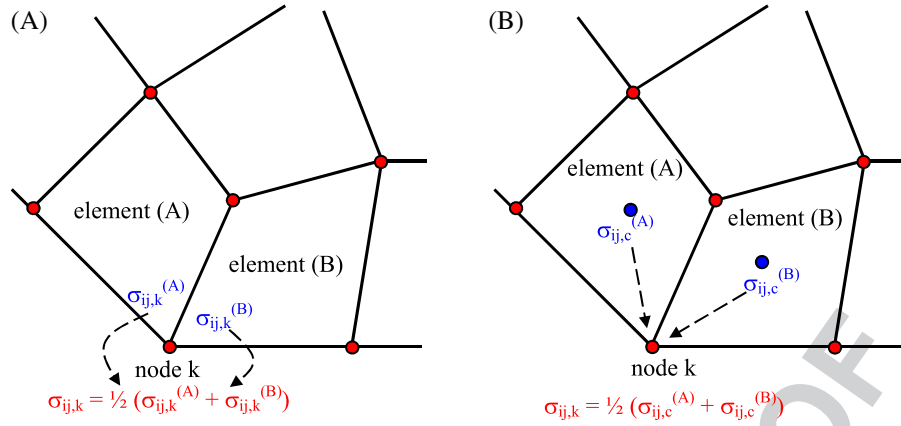


**FIGURE 13** Stress extrapolation at the nodes based on A, nodal stresses or B, centroidal stresses [Colour figure can be viewed at wileyonlinelibrary.com]

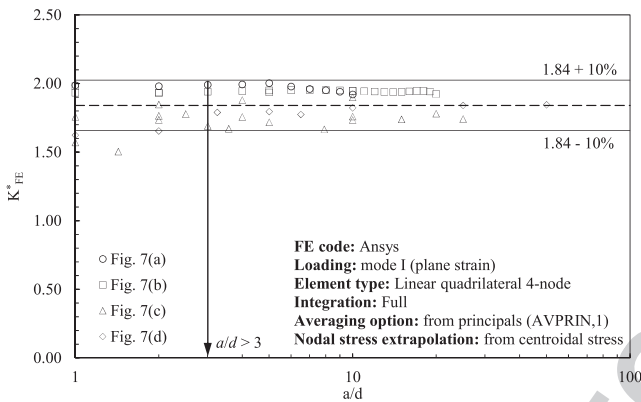


**FIGURE 14** Nondimensional ratio  $K_{FE}^*$  for Ansys FE code. Results for mode I loading based on centroidal stresses (according to Figure 13B)

by adopting one of the following averaging procedures

**F15** (see also Figure 15):

- a. The nodal stress tensors per element ( $[\sigma]_k^{(A)}$  and  $[\sigma]_k^{(B)}$  in Figure 15A) are averaged at the shared node ( $[\sigma]_k$  in Figure 15A), and then nodal principal stresses are calculated ( $\sigma_{11,k}$  is the maximum principal stress in Figure 15A).

- b. The nodal principal stresses per element ( $\sigma_{11,k}^{(A)}$  and  $\sigma_{11,k}^{(B)}$  in Figure 15B) are calculated from the relevant nodal stress tensor per element ( $[\sigma]_k^{(A)}$  and  $[\sigma]_k^{(B)}$  in Figure 15B), and then nodal principal stresses per element are averaged at the shared node ( $\sigma_{11,k}$  in Figure 15B).

Table 6 reports the nomenclature adopted by each FE code to define options (a) and (b) for principal stress averaging. The *default option* is also indicated in the table, and it has been adopted to calibrate the PSM. It should be noted that option (a) is the default for Ansys and Lusas, while option (b) is the default for all other FE codes. This is the reason why averaging option (b) was adopted in Ansys to prepare Figure 14. The different principal stress averaging techniques are one of the reasons for small discrepancies among the results provided by the FE codes: however, such differences are taken up by the scatter band reported in previous Figure 11.

### 8.3 | Finite element mesh pattern

Different mesh patterns were generated by the different FE codes for the same analysed geometry and adopted

**TABLE 6** Options for principal stress averaging available in the considered FE codes

FE Software	Averaging Option (a)	Averaging Option (b)
Ansys	AVPRIN,0 or “from components” ( <i>default</i> )	AVPRIN,1 or “from principals”
Abaqus	“Compute scalars after averaging”	“Compute scalars before averaging” ( <i>default</i> )
Straus 7	<i>Not available</i>	Node average: “Always” ( <i>default</i> )
MSC Patran/Nastran	Average/derive	Derive/average ( <i>default</i> )
Lusas	Averaged nodal ( <i>default</i> )	<i>Not available</i>
Hyperview	Averaging method: “Advanced”	Averaging method: “Simple” ( <i>default</i> )

<sup>a</sup>Postprocessor adopted to calibrate both Optistruct and Ls-Dyna.

Colour online, B&W in print

UNCORRECTED PROOF

59  
60  
61  
62  
63  
64  
65  
66  
67  
68  
69  
70  
71  
72  
73  
74  
75  
76  
77  
78  
79  
80  
81  
82  
83  
84  
85  
86  
87  
88  
89  
90  
91  
92  
93  
94  
95  
96  
97  
98  
99  
100  
101  
102  
103  
104  
105  
106  
107  
108  
109  
110  
111  
112  
113  
114

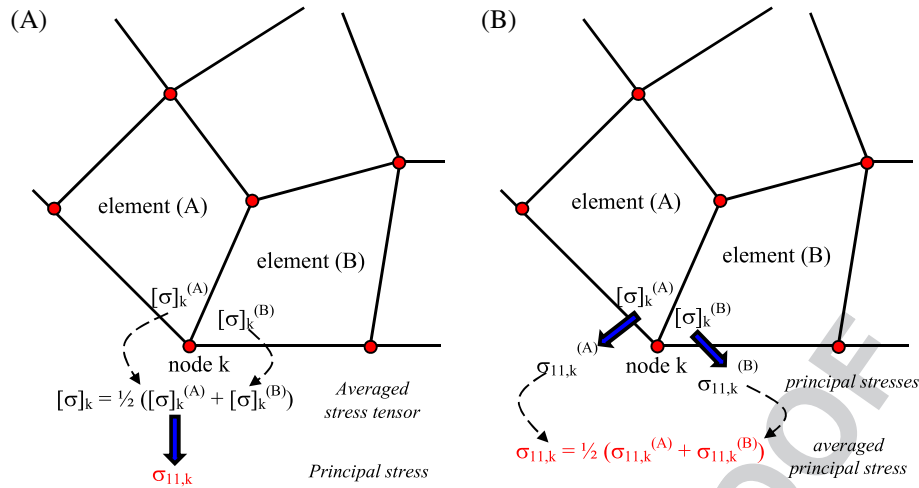


**FIGURE 15** Principal stress averaging options. A, Principal stresses from average stress tensor. B, Principal stresses from element principal stresses [Colour figure can be viewed at wileyonlinelibrary.com]

global element size  $d$ . However, it is worth noting that such differences did not involve the number of elements sharing the node at the V-notch tip, because in all cases the standard pattern prescribed in Figure 2 were obtained, as pointed out previously.

in peak stresses evaluated at the notch tip. Again, stress values obtained by adopting the *default options* (which have been used here to calibrate the PSM) are indicated.

The influence of different mesh patterns was investigated by considering a case study consisting of the mode I problem of Figure 7C with notch depth  $a = 15$  mm, notch opening angle  $2\alpha = 90^\circ$ , and global element size  $d = 1$  mm. The FE meshes generated by a selection of FE codes, namely Ansys, Abaqus, and MSC Patran/Nastran, are reported in Table 7 along with the results

Table 7 allows to quantify the effect of different mesh patterns (in shape and arrangement of the elements) on the peak stress values for the same principal stress averaging option. However, in the context of the present round robin, comparison among the 3 FE codes should not be made for the same averaging option, but rather for the default option of each FE code. It is seen that the differences among the calculated stresses (6.309, 6.093, and

**TABLE 7** FE mesh patterns relevant to the case of Figure 7c with  $a = 15$  mm,  $2\alpha = 90^\circ$ , and  $d = 1$  mm, as obtained with different FE codes

Ansyes	Abaqus	MSC Patran/Natran
$\sigma_{yy,peak}/\sigma_{nom} = 6.185$	$\sigma_{yy,peak}/\sigma_{nom} = 5.833$	$\sigma_{yy,peak}/\sigma_{nom} = 6.092$
$\sigma_{I,peak}/\sigma_{nom} = 6.309$ (default) averaging option (a)	$\sigma_{I,peak}/\sigma_{nom} = 5.918$ averaging option (a)	$\sigma_{I,peak}/\sigma_{nom} = 6.183$ averaging option (a)
$\sigma_{I,peak}/\sigma_{nom} = 6.514$ averaging option (b)	$\sigma_{I,peak}/\sigma_{nom} = 6.093$ (default) averaging option (b)	$\sigma_{I,peak}/\sigma_{nom} = 6.386$ (default) averaging option (b)

Results in peak stresses evaluated at the notch tip. Peak stress values obtained by adopting the *default options*, which have been used to calibrate PSM, are indicated.

Colour online, B&W in print

58  
59  
60  
61  
62  
63  
64  
65  
66  
67  
68  
69  
70  
71  
72  
73  
74  
75  
76  
77  
78  
79  
80  
81  
82  
83  
84  
85  
86  
87  
88  
89  
90  
91  
92  
93  
94  
95  
96  
97  
98  
99  
100  
101  
102  
103  
104  
105  
106  
107  
108  
109  
110  
111  
112  
113  
114

6.386 in Ansys, Abaqus, and MSC Patran/Nastran, respectively) is reduced and it is included in the scatter bands reported in Figure 11.

### 8.4 | Numerical integration scheme

Each FE software provides different integration scheme options for the same element type, which typically cover full and reduced integrations, but, optionally, include also some enhanced formulations that allow to avoid numerical errors, associated to shear locking, hourglass effect, and volumetric locking.

To investigate the effect of different integration schemes, the 2D mode I problem of Figure 7C with notch depth  $a = 15$  mm, notch opening angle  $2\alpha = 90^\circ$ , and global element size  $d = 1$  mm was considered again as a case study. To exclude the effect of the mesh pattern, an FE mesh has been generated in Ansys by using the free mesh generation algorithm (see Figure 16), and afterwards, it has been imported into all FE codes involved in the present round robin. By doing so, identical mesh patterns have been used with different FE codes. All available options associated to a  $2 \times 2$  Gauss point integration scheme have been adopted in each FE code.

The results in peak stresses evaluated at the notch tip are reported in Tables 8 and 9, where *default options* are indicated. Table 8 lists the results calculated with FE codes that use Equation 10 to evaluate nodal stresses, while Table 9 reports the stress values calculated by FE codes that adopt Equation 11. In Table 9, results from Ansys and Straus 7 have been included for comparison purposes: it is worth noting that all calculations were made by hand, because Ansys and Straus 7 do not implement stress averaging at FE nodes when stresses at

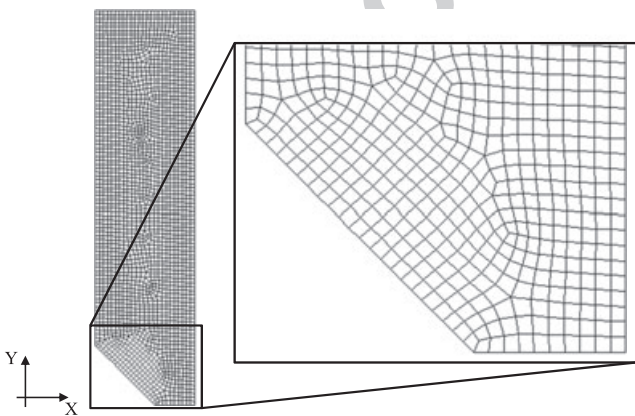


**FIGURE 16** FE mesh pattern relevant to case 7c with  $a = 15$  mm,  $2\alpha = 90^\circ$ , and  $d = 1$  mm, as obtained by means of Ansys free mesh generation algorithm

**TABLE 8** Peak stresses evaluated at the V-notch tip by using the mesh pattern of Figure 16

Software	Ansys	Abaqus	Straus 7	Patran/Nastran	Lusas
Element type	Plane 182	CPE4I	QUAD4	CQUAD4	QPN4M
Integration	Simple Enh. strain $2 \times 2$	Full $2 \times 2$	Incimp. modes $2 \times 2$	Standard formulation $2 \times 2$	Full with Enh. strain $2 \times 2$
Stress state	Plane strain	Plane strain	Plane strain	Plane strain	Plane strain
$\sigma_{yy,peak}/\sigma_{nom}$	6.185	6.260	6.120	6.185	6.227
$\sigma_{I,peak}/\sigma_{nom}$ averaging option (a)	6.309 (default)	6.386	n.a.	6.309	6.312 (default)
$\sigma_{I,peak}/\sigma_{nom}$ averaging option (b)	6.514	6.590	6.445 (default)	6.514 (default)	6.492

Results based on nodal stresses (according to Equation 10 and Figure 13A). Peak stress values obtained by adopting *default options* are indicated.

58  
59  
60  
61  
62  
63  
64  
65  
66  
67  
68  
69  
70  
71  
72  
73  
74  
75  
76  
77  
78  
79  
80  
81  
82  
83  
84  
85  
86  
87  
88  
89  
90  
91  
92  
93  
94  
95  
96  
97  
98  
99  
100  
101  
102  
103  
104  
105  
106  
107  
108  
109  
110  
111  
112  
113  
114



**TABLE 9** Peak stresses evaluated at the V-notch tip by using the mesh pattern of Figure 16

Software	Hypermesh/Ls-Dyna/ Hyperview	Hypermesh/Optistruct/ Hyperview	Ansys			Straus 7
Element type	Shell 4 node, Element formulation 13	Shell CQUAD4	Plane 182			QUAD4
Integration	<i>n.a.</i>	<i>n.a.</i>	Simple Enh. strain	Enh. strain	Full	Incomp. modes
Gauss points	2 × 2	2 × 2	2 × 2			2 × 2
Stress state	Plane strain	Plane strain	Plane strain			Plane strain
$\sigma_{yy,peak}/\sigma_{nom}$	4.770	4.743	4.720	4.720	4.781	4.718
$\sigma_{I,peak}/\sigma_{nom}$ averaging option (a)	4.898	4.874	4.840	4.840	4.910	<i>n.a.</i>
$\sigma_{I,peak}/\sigma_{nom}$ averaging option (b)	5.019 ( <i>default</i> )	5.003 ( <i>default</i> )	4.962	4.962	5.031	4.965

Results based on centroidal stresses (according to Equation 11 and Figure 13B). Peak stress values obtained by adopting *default options* are indicated.

element centroids are used. Table 8 shows the perfect match of the fully integrated elements between Ansys and Abaqus. Moreover, the simple enhanced strain formulation in Ansys, adopted to perform the original calibration of the PSM,<sup>22</sup> fully agrees with the standard formulation of MSC Patran/Nastran. Table 9 shows the excellent agreement of Hypermesh/Optistruct/Hyperview and Hypermesh/Ls-Dyna/Hyperview software packages with the fully integrated plane elements of Ansys. This is the reason why full integration was adopted in Ansys to compile previous Figure 14.

The different integration scheme options adopted by the different FE packages are a further source of scatter of results; however, all of them are taken up by the proposed scatter bands.

It is interesting to note that some commercial FE codes, other than those considered here, provide the full integration scheme as the *default* setting (an example of these codes is Adina®), or even as the sole option (an example of these codes is Sysweld®). Therefore, calibrating the PSM by adopting this formulation might be useful. To this aim, mode I analyses have been repeated by adopting Ansys and Abaqus FE codes, by adopting the full integration scheme, Equation 10 to extrapolate nodal stresses, and the averaging option (b) (see Figure 15B) to calculate principal stresses. The results are reported in Figure 17, and it is seen that both FE codes converge to the value  $K_{FE}^* \cong 1.55$ . However, a slightly greater scatter band of  $\pm 8\%$  should be accepted for Abaqus (Figure 17B) as compared to  $\pm 5\%$  valid for Ansys (Figure 17A). This difference can be explained on the basis of the different local mesh patterns generated by Ansys and Abaqus FE codes: 2 examples are highlighted inside Figure 17A,B, which show that the free

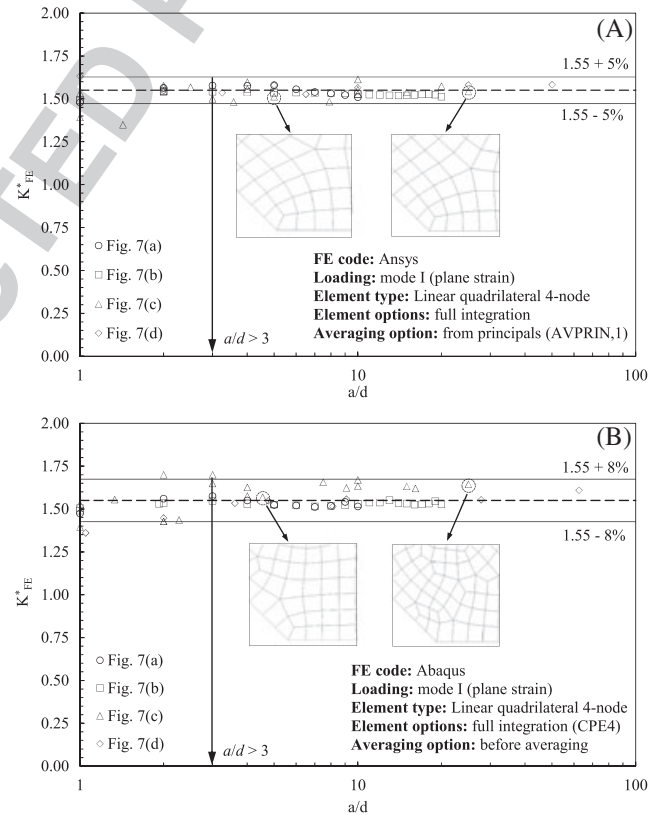


**FIGURE 17** Nondimensional ratio  $K_{FE}^*$  for A, Ansys and B, Abaqus FE codes. Results for mode I loading obtained by activating the full integration scheme and by adopting the principal stress averaging option of Figure 15B

mesh generation algorithm of Ansys provides very similar mesh patterns for the 2 cases; differently, Abaqus provides quite different mesh patterns for the same cases, giving rise to a slightly increased scattering of results.

Finally, it should be noted that for both Ansys and Abaqus FE codes, the convergence is guaranteed for a mesh density ratio  $a/d > 3$ , such value being consistent with previous calibrations reported in Figure 11.

## 9 | CONCLUSIONS

A round robin has been carried out to calibrate the PSM to rapidly estimate the linear elastic NSIF parameters relevant to mode I and mode II loadings. Different commercial FE codes and a range of coarse mesh patterns have been used. Essentially, the PSM is a simplified, FE-oriented numerical technique originally calibrated by using Ansys software, which takes the singular, linear elastic peak stresses calculated at the point of singularity with coarse FE meshes to estimate the mode I NSIF and the mode II SIF. Two calibration constants are needed, namely  $K_{FE}^*$  (Equation 3) and  $K_{FE}^{**}$  (Equation 4), respectively, which have been calibrated in this paper for 4-node quadrilateral FEs with linear shape functions available in some FE software packages, other than Ansys. The following conclusions can be drawn from the present study:

- Dealing with mode I loading, FE codes that extrapolate nodal stresses per element from stresses at the integration points, namely Ansys, Abaqus, Straus 7, MSC Patran/Nastran, and Lusas, exhibit the same calibration constant, ie,  $K_{FE}^* \cong 1.38$ , as originally found for Ansys software. Finite element results fall within a scatter band of  $\pm 5\%$  when the mesh density ratio  $a/d$  is equal to or greater than 3. On the other hand, FE codes that attribute the centroidal stress to the element nodes, namely Hypermesh/Optistruct/Hyperview and Hypermesh/Ls-Dyna/Hyperview, present a different value, ie,  $K_{FE}^* \cong 1.84$ . In this case, FE results were seen to fall in a slightly wider scatter band of  $\pm 8\%$ , when the mesh density ratio is again  $a/d \geq 3$ .
- Dealing with mode II loading, all FE codes involved in the round robin present the same calibration constant independently of the nodal stress extrapolation procedure, ie,  $K_{FE}^{**} \cong 3.38$  with a scatter band of  $\pm 3\%$  for a mesh density ratio  $a/d \geq 14$ . All these results are consistent with the original calibration of Ansys software.
- The effects of principal stress averaging options, mesh patterns, and element formulation settings have been investigated. In summary, when adopting the *default options* of each software, the influences of all previous analysis features are taken up by the scatter bands of  $\pm 5\%$  or  $\pm 8\%$  defined for the calibration constant  $K_{FE}^*$  and  $\pm 3\%$  valid for  $K_{FE}^{**}$ .
- As a side result, Ansys and Abaqus were run also by setting fully integrated, 4-node elements, nodal stress

extrapolation from integration points, and principal stress averaging from principals. These settings are the default ones for existing FE packages other than those analysed in the present work. The result obtained was  $K_{FE}^* \cong 1.55$  with a scatter band of  $\pm 5\%$  for Ansys and of  $\pm 8\%$  for Abaqus, provided that the mesh density ratio  $a/d$  is equal to or greater than 3.

## ACKNOWLEDGEMENTS

The round robin was conceived and conducted by the Working Group on “Joining Techniques” of the Italian Scientific Association for Stress Analysis (AIAS). The precious effort of all participants is gratefully acknowledged.

## ORCID

G. Meneghetti  <http://orcid.org/0000-0002-4212-2618>

A. Campagnolo  <http://orcid.org/0000-0001-8685-6210>

## REFERENCES

1. Williams ML. Stress singularities resulting from various boundary conditions in angular corners of plates in tension. *J Appl Mech.* 1952;19:526-528.
2. Gross B, Mendelson A. Plane elastostatic analysis of V-notched plates. *Int J Fract Mech.* 1972;8(3):267-276.
3. Lazzarin P, Zambardi R. A finite-volume-energy based approach to predict the static and fatigue behavior of components with sharp V-shaped notches. *Int J Fract.* 2001;112(3):275-298.
4. Dunn ML, Suwito W, Cunningham S, May CW. Fracture initiation at sharp notches under mode I, mode II, and mild mixed mode loading. *Int J Fract.* 1997;84(4):367-381.
5. Fett T. Failure of brittle materials near stress singularities. *Eng Fract Mech.* 1996;53(4):511-518.
6. Gómez FJ, Elices M. A fracture criterion for sharp V-notched samples. *Int J Fract.* 2003;123(3/4):163-175.
7. Nui LS, Chehimi C, Pluvina G. Stress field near a large blunted tip V-notch and application of the concept of the critical notch stress intensity factor (NSIF) to the fracture toughness of very brittle materials. *Eng Fract Mech.* 1994;49(3):325-335.
8. Planas J, Elices M, Guinea G, Gómez F, Cendón D, Arbillá I. Generalizations and specializations of cohesive crack models. *Eng Fract Mech.* 2003;70(14):1759-1776.
9. Seweryn A. Brittle fracture criterion for structures with sharp notches. *Eng Fract Mech.* 1994;47(5):673-681.
10. Boukharouba T, Tamine T, Niu L, Chehimi C, Pluvina G. The use of notch stress intensity factor as a fatigue crack initiation parameter. *Eng Fract Mech.* 1995;52(3):503-512.
11. Kihara S, Yoshii A. A strength evaluation method of a sharply notched structure by a new parameter, “The equivalent stress

- intensity factor'. *JSME Int J Ser 1, S Mech Str Mater*. 1991;34:70-75.
12. Atzori B, Meneghetti G. Fatigue strength of fillet welded structural steels: finite elements, strain gauges and reality. *Int J Fatigue*. 2001;23(8):713-721.
  13. Lazzarin P, Livieri P. Notch stress intensity factors and fatigue strength of aluminium and steel welded joints. *Int J Fatigue*. 2001;23(3):225-232.
  14. Lazzarin P, Tovo R. A notch intensity factor approach to the stress analysis of welds. *Fatigue Fract Eng Mater Struct*. 1998;21(9):1089-1103.
  15. Lazzarin P, Lassen T, Livieri P. A notch stress intensity approach applied to fatigue life predictions of welded joints with different local toe geometry. *Fatigue Fract Eng Mater Struct*. 2003;26(1):49-58.
  16. Livieri P, Lazzarin P. Fatigue strength of steel and aluminium welded joints based on generalised stress intensity factors and local strain energy values. *Int J Fract*. 2005;133(3):247-276.
  17. Verreman Y, Nie B. Early development of fatigue cracking at manual fillet welds. *Fatigue Fract Eng Mater Struct*. 1996;19(6):669-681.
  18. Lazzarin P, Sonsino CM, Zambardi R. A notch stress intensity approach to assess the multiaxial fatigue strength of welded tube-to-flange joints subjected to combined loadings. *Fatigue Fract Eng Mater Struct*. 2004;27(2):127-140.
  19. Nisitani H, Teranishi T.  $K_I$  value of a circumferential crack emanating from an ellipsoidal cavity obtained by the crack tip stress method in FEM. In: Guagliano M, Aliabadi MH (eds) *Proceedings of the 2nd international conference on fracture and damage mechanics*. 2001;141-146.
  20. Nisitani H, Teranishi T.  $K_I$  of a circumferential crack emanating from an ellipsoidal cavity obtained by the crack tip stress method in FEM. *Eng Fract Mech*. 2004;71(4-6):579-585.
  21. Meneghetti G, Guzzella C. The peak stress method to estimate the mode I notch stress intensity factor in welded joints using three-dimensional finite element models. *Eng Fract Mech*. 2014;115:154-171.
  22. Meneghetti G, Lazzarin P. Significance of the elastic peak stress evaluated by FE analyses at the point of singularity of sharp V-notched components. *Fatigue Fract Eng Mater Struct*. 2007;30(2):95-106.
  23. Meneghetti G. The use of peak stresses for fatigue strength assessments of welded lap joints and cover plates with toe and root failures. *Eng Fract Mech*. 2012;89:40-51.
  24. Meneghetti G. The peak stress method for fatigue strength assessment of tube-to-flange welded joints under torsion loading. *Weld World*. 2013;57(2):265-275.
  25. Bertini L, Frendo F, Marulo G. Effects of plate stiffness on the fatigue resistance and failure location of pipe-to-plate welded joints under bending. *Int J Fatigue*. 2016;90:78-86.
  26. Cosso GL, Rizzo CM, Servetto C. Fitness-for-service assessment of defected welded structural details by experimental evaluation of the fatigue resistance S-N curve. *Weld World*. 2016;60(5):847-858.
  27. Fischer C, Fricke W, Meneghetti G, Rizzo C. Fatigue strength assessment of HP stiffener joints with fillet-welded attachments using the peak stress method. In: Brinkmann B, Wriggers P (eds) *Proc. 5th Int. Conf. Computational Methods in Marine Engineering MARINE 2013*. Hamburg (D), 2013.
  28. Ranieri S, Rizzo CM, Cosso GL, Servetto C. Metodi avanzati per la verifica a fatica di giunti saldati di testa. *Xxx*. 2015;67:501-511. (in Italian) Q3
  29. Ferro P, Colussi M, Meneghetti G, Berto F, Lachin M, Castiglione SA. On the use of the peak stress method for the calculation of residual notch stress intensity factors: a preliminary investigation. *Procedia Struct Integr*. 2017;3:191-200.
  30. Ouchida H, Nishioka A. A study of fatigue strength of fillet welded joints. In: *IIW Doc. XIII-338-64*, 1964.
  31. Meneghetti G, Lazzarin P. The peak stress method for fatigue strength assessment of welded joints with weld toe or weld root failures. *Weld World*. 2011;55(7-8):22-29.

**How to cite this article:** Meneghetti G, Campagnolo A, Avalle M, et al. Rapid evaluation of notch stress intensity factors using the peak stress method: Comparison of commercial finite element codes for a range of mesh patterns. *Fatigue Fract Eng Mater Struct*. 2017;1-20. <https://doi.org/10.1111/ffe.12751>

## APPENDIX A

### DETAILS OF MESH GENERATION SETTINGS

In the following, details concerning element type/options along with the adopted mesh generation settings are reported for each FE code:

- Ansys
  - Element type: Solid → Quad 4-node (PLANE 42 or PLANE 182)
  - Element options: Plane strain, Simple enhanced strain (only for PLANE 182)
  - Element size: Size Cntrls → Manual Size → Global → Size =  $d$
  - Mesh generation: Mesh → Areas → Free
- Abaqus
  - Element type: Standard → linear → Quad
  - Element options: Plane strain, Incompatible modes (CPE4I)
  - Element size: Global Seeds → Sizing Cntrls → Approximate global size =  $d$
  - Mesh generation: Mesh Cntrls → Free → Advancing front → “Use mapped meshing where appropriate” MUST BE INACTIVE; Mesh Part Instance → Ok

- Straus 7
  - Element type: linear 4-node quadrilateral plate (QUAD4)
  - Element options: Plane strain
  - Element size: Automeshing → Surface mesh → Sizes → Maximum edge length =  $d$
  - Mesh generation: Automeshing → Surface mesh → Mesh
- MSC Patran/Nastran
  - Element type: 2D Solid (CQUAD4)
  - Element options: Plane strain, Standard formulation
  - Element size: Mesh → Surface → Global Edge Length → Value =  $d$
  - Mesh generation: Mesh → Surface → Elem Shape → Quad; Mesher → Paver; Topology → Quad4
- Lusas
  - Element type: 2D continuum element with enhanced strains (QPN4M)
  - Element options: Plane strain, Quadrilateral, Linear interpolation
  - Element size: Mesh → Surface Mesh → Irregular mesh → Element size =  $d$
  - Mesh generation: Mesh → Surface Mesh
- Hypermesh/Optistruct/Hyperview
  - Element type: Shell 4-node (*Hypermesh*), CQUAD4 (*Optistruct*)
  - Element options: MID2 = -1 (plane strain), MID3 = blank (*Optistruct*)
  - Element size: Mesh → Surfs → Size and bias → Element size =  $d$  (*Hypermesh*)
  - Mesh generation: Mesh → Surfs → Mesh type → quads; mesh (*Hypermesh*)
- Hypermesh/Ls-Dyna/Hyperview
  - Element type: Shell 4-node (*Hypermesh*)

Element options: Element formulation 13 (Plane strain x-y plane) (*LS-Dyna*)

Element size: Mesh → Surfs → Size and bias-Element size =  $d$  (*Hypermesh*)

Mesh generation: Mesh → Surfs → Mesh type-quads; mesh (*Hypermesh*)

## APPENDIX B

### DEFAULT OPTIONS OF THE POSTPROCESSING ENVIRONMENT

The *default options* of the post-processing environment of each FE code considered here are listed in the following:

- Ansys
  - Options for outputs: Principal stress calcs → from components (or equivalently AVPRIN = 0)
- Abaqus
  - Result options: Averaging → Compute order → Compute scalars before averaging → Averaging threshold = 100%
- Straus 7
  - Node average: Always
- MSC Patran/Nastran
  - Averaging definition: Method → Derive/Average
- Lusas
  - Properties: Value results → Location → Averaged nodal
- Hypermesh/Optistruct/Hyperview
  - Averaging method: Simple
- Hypermesh/Ls-Dyna/Hyperview
  - Averaging method: Simple.

UNCORRECTED PROOF